Split-component PML absorbing conditions for SS-TLM

Sandrick Le Maguer, Michel Ney

Split-component PML absorbing conditions for SS-TLM

S. Le Maguer*,† and M. M. Ney

GET/ENST Bretagne/Département MO, CNRS LEST (Laboratory of Electronics and Systems for Telecommunications), CS 83818, 29238 BREST Cedex 3, France

Known as alternate direct implicit (ADI) or split-step (SS) schemes, a new class of time-domain algorithms has recently been proposed. Their salient feature concerns their numerical stability, regardless the time-step used. Thus, significant computational advantages can be obtained when non-uniform mesh is used. To study open structures or determine S-parameters, absorbing boundary conditions (ABC) have to be used. The perfectly matched layers (PML) technique based on split field component is implemented for the SS-TLM algorithm. The complete set of updating equations is provided and the new PML is validated. It is shown to provide high accuracy even better than that of classical PML-TLM scheme. In addition, it is found that using a high time-step does not seem to degrade significantly the accuracy of PML. Thus, the PML technique is very well adapted to SS-TLM as confirmed by various applications. Finally, unlike all classical TLM-PML schemes, the technique is found to be stable.

KEY WORDS: transmission line matrix (TLM); split step (SS); unconditional stability; absorbing boundary conditions (ABC); perfectly matched layers (PML); antenna

1. INTRODUCTION

Full-wave electromagnetic modelling has become a required step towards the design of RF, microwave and millimetre-wave passive and active components. Indeed, it has become the essential tool for optimizing structures and circuits in some rigorous manner and hence, reducing the design time. However, as models are based on Maxwell's field equations, the computer cost required is still very high and generally this prevents the use of such models directly in an optimization procedure.

The current challenge is to develop new numerical procedures that can speed up simulation time for relatively complex structures. Hence, time-domain volumic methods such as FDTD, TLM, etc. have attracted researchers' attention and have undergone some substantial development during recent years. Rather known as slow numerical procedures they benefit from the constant increase of computer power. However, this is compensated by the increase of

*Correspondence to: S. Le Maguer, GET/ENST Bretagne/Département MO, CNRS LEST (Laboratory of Electronics and Systems for Telecommunications), CS 83818, 29238 BREST Cedex 3, France.
† E-mail: sandrick.lemaguer@enst-bretagne.fr

systems complexity. In addition, constraints on the time-step due to mesh refinement that is required to reduce coarseness error, still constitutes a drawback for these methods.

As a result, new algorithms known as ADI 'Alternate Direction Implicit' [1, 2] or SS 'Split-Step' [3, 4] have been recently proposed. They have the advantage to alleviate the constraint on the maximum usable time-step. This property provides some very important advantage when using irregular meshing. However, if they are unconditionally stable, time-step is an important parameter that has some impact on the algorithm velocity error [3]. But when irregular meshing is used, one order of magnitude reduction in computer cost can be obtained [4].

Although some work was presented on SS-TLM [3, 4], theoretical foundation of the basic algorithm is still required. In addition, other required procedures such as absorbing boundary conditions (ABC) have to be developed. These conditions are necessary for structures open to free-space (antenna, RCS) or for S-parameter computation. The objective of the paper is to present a PML-type ABC for the new SS-TLM algorithm.

2. SS-TLM BASIC ALGORITHM

SS-TLM algorithm is based on a modification of the time-sampling procedure in Maxwell's field curl equations. Unlike the basic TLM scheme, the technique splits the basic equations into two successive steps. For instance, the time-dependence of the x-electric field component E_x, Maxwell–Ampere relation is divided into two sub-equations:

$$\frac{1}{2}\left(\varepsilon_x\varepsilon_0\frac{\partial E_x}{\partial t}+\sigma_{\mathrm{ex}}E_x\right)=\frac{\partial H_z}{\partial y} \tag{1}$$

$$\frac{1}{2}\left(\varepsilon_x\varepsilon_0\frac{\partial E_x}{\partial t}+\sigma_{\mathrm{ex}}E_x\right)=-\frac{\partial H_y}{\partial z} \tag{2}$$

where ε_0 the permittivity of free space, ε_x the relative permittivity in the x-direction and σ_{ex} the electric conductivity in the same direction. According to the theory of split algorithms [5], Equations (1) and (2) have to be solved one after the other in the iterative process to obtain an unconditionally stable algorithm. Furthermore, to get a coherent spatial mapping of field components the scheme is divided in two-steps as follows: the first step is obtained by an approximation of Equation (1) between $(n-\frac{1}{2})\Delta t$ and $n\Delta t$ (Δt being the time-step) and an approximation of Equation (2) between $n\Delta t$ and $(n+\frac{1}{2})\Delta t$. The second step is obtained by an approximation of Equation (2) between $(n+\frac{1}{2})\Delta t$ and $(n+1)\Delta t$ and an approximation of Equation (1) between $(n+1)\Delta t$ and $(n+\frac{3}{2})\Delta t$. These approximations are performed using the approach proposed by Peña and Ney [6].

However, unlike basic TLM algorithm, SS-TLM is no longer purely explicit. It includes an initial implicit solution which is solved by matrix inversion. This procedure must be performed once before the time-iteration procedure begins. The overtime brought by the implicit procedure is, generally, largely compensated by the gain when irregular meshing is used. Indeed, the time-step enforced by the smallest mesh size with the non-split algorithm can be chosen the same as the one related to the largest cell with SS-TLM. By using this adequate meshing strategy [3, 4], substantial reduction in terms of computer cost can be achieved for comparable accuracy.

Furthermore, only the six fields components at the centre of the cell need to be stored. Thus, a memory gain of a factor 3 is obtained compared to the classical TLM scheme (SCN).

3. PML BOUNDARIES

3.1. PML formulation

Much work has been reported on ABC for TLM computation. For instance, PML [7], generally recognized as the most efficient technique, was reported with implementation in TLM-SCN [8]. It can be mentioned that, because of the presence of parasitic modes generated by the SCN scheme, some stability problem was reported. However, an interesting observation can be made from the dispersion analysis of SS-TLM node: No parasitic solutions were found [9]. Consequently, it is expected that the PLM scheme when implemented in the SS-TLM algorithm will not produce any instabilities.

The implementation of the so-called PML may be carried out using several formulations: the PML split components originally proposed by Bérenger [7] and the PML 'unsplit' approach proposed by Gedney [10]. Since an extended version of the first approach is already available with TLM [8], this technique has been chosen to be first implemented in SS-TLM. Thus, consistent comparison between SS-TLM and TLM can be shown.

In the PML layer, field components are split into two sub-components. For instance considering E_x field components:

$$E_x = E_{xy} + E_{xz} \tag{3}$$

The time-domain evolution of these sub-components is governed by the following equations:

$$\varepsilon_x \varepsilon_0 \frac{\partial E_{xy}}{\partial t} + \sigma_{ey} E_{xy} = \frac{1}{\alpha_y} \frac{\partial H_z}{\partial y} \tag{4}$$

$$\varepsilon_x \varepsilon_0 \frac{\partial E_{xz}}{\partial t} + \sigma_{ez} E_{xz} = -\frac{1}{\alpha_z} \frac{\partial H_y}{\partial z} \tag{5}$$

where σ_{ey} is a new electrical conductivity in (oy) direction (propagating waves absorption) and α_y a coefficient greater than unity (evanescent waves damping in the same direction).

3.2. SS-TLM implementation

The implementation for SS-TLM computation is not straightforward. Equations (4) and (5) need to be split as shown with Equation (1) and (2). But, as only one space derivative is present in the right-hand side of (4) and (5) instead of two for Maxwell equations a problem arises. The only solution is to split Equation (4) as follows:

$$\frac{1}{2}\left(\varepsilon_x \varepsilon_0 \frac{\partial E_{xy}}{\partial t} + \sigma_{ey} E_{xy}\right) = \frac{1}{\alpha_y} \frac{\partial H_z}{\partial y} \tag{6}$$

$$\frac{1}{2}\left(\varepsilon_x \varepsilon_0 \frac{\partial E_{xy}}{\partial t} + \sigma_{ey} E_{xy}\right) = 0 \tag{7}$$

Equation (5) is split using the same technique:

$$\frac{1}{2}\left(\varepsilon_x \varepsilon_0 \frac{\partial E_{xz}}{\partial t} + \sigma_{ez} E_{xz}\right) = -\frac{1}{\alpha_z} \frac{\partial H_y}{\partial z} \tag{8}$$

$$\frac{1}{2}\left(\varepsilon_x \varepsilon_0 \frac{\partial E_{xz}}{\partial t} + \sigma_{ez} E_{xz}\right) = 0 \tag{9}$$

To keep the same spatial mapping of fields than with SS-TLM, one needs to solve first (6) and (9), then (7) and (8). The resulting scheme is very similar to the classical SS-TLM one. Only few impedance terms are changed in the matrices involved in the implicit process. For instance, if Δt is the time-step, one can approximate (7) and (8) using the technique described in Reference [4], and the TLM space discretization depicted in Figure 1. If this approximation is enforced between $n\Delta t$ and $(n+\frac{1}{2})\Delta t$, one can easily obtain:

$$2\Delta x E_{xz}^{(n)} = A'_{\mathrm{ex}z}[(\Delta x E_2^{xz} - Z_{\mathrm{ex}z}\Delta y H_2^y) + (\Delta x E_9^{xz} + Z_{\mathrm{ex}z}\Delta y H_9^y)]^{(n+1/2)} \tag{10}$$

and:

$$2\Delta x E_{xy}^{(n)} = A'_{\mathrm{ex}y}[\Delta x E_2^{xy} + \Delta x E_9^{xy}]^{(n+1/2)} \tag{11}$$

with:

$$A'_{\mathrm{ex}y} = \frac{4}{4 - Z_0 s(\sigma_{\mathrm{e}y}/\varepsilon_x)}, \quad Z_{\mathrm{ex}z} = Z_0 \frac{s\Delta x}{\varepsilon_x \alpha_z \Delta y \Delta z}, \quad s = 2c_0\Delta t$$

where Δx, Δy and Δz are the cell dimension and Z_0 the impedance of free space. Field components subscripts from the right-hand part of (10) and (11) correspond to port numbers as defined by Johns [11]. Thus, by adding (10) and (11) and using the property described in (3) yields to:

$$\frac{2\Delta x E_{xz}^{(n)}}{A'_{\mathrm{ex}z}} + \frac{2\Delta x E_{xy}^{(n)}}{A'_{\mathrm{ex}y}} = [(\Delta x E_2^x - Z_{\mathrm{ex}z}\Delta y H_2^y) + (\Delta x E_9^x + Z_{\mathrm{ex}z}\Delta y H_9^y)]^{(n+1/2)} \tag{12}$$

This expression can be compared to the corresponding equation of the non-PLM SS-TLM scheme:

$$\frac{2\Delta x E_x^{(n)}}{A'_{\mathrm{ex}}} = [(\Delta x E_2^x - Z_{\mathrm{ex}}\Delta y H_2^y) + (\Delta x E_9^x + Z_{\mathrm{ex}}\Delta y H_9^y)]^{(n+1/2)} \tag{13}$$

with:

$$A'_{\mathrm{ex}} = \frac{4}{4 - Z_0 s(\sigma_{\mathrm{ex}}/\varepsilon_x)} \quad \text{and} \quad Z_{ex} = Z_0 \frac{s\Delta x}{\varepsilon_x \Delta y \Delta z}$$

As expected the only change in the right-hand side is the impedance Z_{ex} which is replaced by $Z_{\mathrm{ex}z}$. Then, the implementation of the PML scheme in a SS-TLM code is straightforward. The complete set of updating equations is presented in Tables I and II. Finally, 12 field sub-

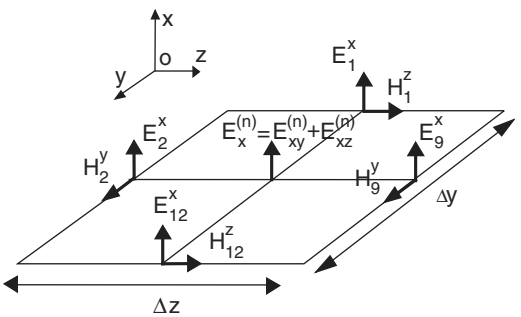

Figure 1. SS-TLM fields samples in the (*yoz*) plane with respect to Johns' notation [11].

Table I. Summary of PML SS-TLM updating equations for step 1.

Explicit part (from $(n-\frac{1}{2})\Delta t$ to $n\Delta t$)	
$\frac{2\Delta x E_{xy}^{(n)}}{A_{exy}} + \frac{2\Delta x E_{xz}^{(n)}}{A_{exz}} = [(\Delta x E_1^x - Z_{exy}\Delta z H_1^z) + (\Delta x E_{12}^x + Z_{exy}\Delta z H_{12}^z)]^{(n-1/2)}$	$\frac{2\Delta x E_{xz}^{(n)}}{A_{exz}} = \frac{2\Delta x E_{xz}^{(n-1)}}{A'_{exz}}$
$\frac{2\Delta y E_{yz}^{(n)}}{A_{eyz}} + \frac{2\Delta y E_{yx}^{(n)}}{A_{eyx}} = [(\Delta y E_4^y - Z_{eyz}\Delta x H_4^x) + (\Delta y E_8^y + Z_{eyz}\Delta x H_8^x)]^{(n-1/2)}$	$\frac{2\Delta y E_{yx}^{(n)}}{A_{eyx}} = \frac{2\Delta y E_{yx}^{(n-1)}}{A'_{eyx}}$
$\frac{2\Delta z E_{zx}^{(n)}}{A_{ezx}} + \frac{2\Delta z E_{zy}^{(n)}}{A_{ezy}} = [(\Delta z E_6^z - Z_{ezx}\Delta y H_6^y) + (\Delta z E_{10}^z + Z_{ezx}\Delta y H_{10}^y)]^{(n-1/2)}$	$\frac{2\Delta z E_{zy}^{(n)}}{A_{ezy}} = \frac{2\Delta z E_{zy}^{(n-1)}}{A'_{ezy}}$
$2Z_0\frac{\Delta x H_{xz}^{(n)}}{\bar{D}_{xz}A_{mxz}} + \frac{Z_{mxz}}{Z_{mxy}}2Z_0\frac{\Delta x H_{xy}^{(n)}}{\bar{D}_{xy}A_{mxy}} = [(\Delta y E_8^y + Z_{mxz}\Delta x H_8^x) - (\Delta y E_4^y - Z_{mxz}\Delta x H_4^x)]^{(n-1/2)}$	$2Z_0\frac{\Delta x H_{xy}^{(n)}}{\bar{D}_{xy}A_{mxy}} = 2Z_0\frac{\Delta x H_{xy}^{(n-1)}}{\bar{D}_{xy}A'_{mxy}}$
$2Z_0\frac{\Delta y H_{yx}^{(n)}}{\bar{D}_{yx}A_{myx}} + \frac{Z_{myx}}{Z_{myz}}2Z_0\frac{\Delta y H_{yz}^{(n)}}{\bar{D}_{yz}A_{myz}} = [(\Delta z E_{10}^z + Z_{myx}\Delta y H_{10}^y) - (\Delta z E_6^z - Z_{myx}\Delta y H_6^y)]^{(n-1/2)}$	$2Z_0\frac{\Delta y H_{yz}^{(n)}}{\bar{D}_{yz}A_{myz}} = 2Z_0\frac{\Delta y H_{yz}^{(n-1)}}{\bar{D}_{yz}A'_{myz}}$
$2Z_0\frac{\Delta z H_{zy}^{(n)}}{\bar{D}_{zy}A_{mzy}} + \frac{Z_{mzy}}{Z_{mzx}}2Z_0\frac{\Delta z H_{zx}^{(n)}}{\bar{D}_{zx}A_{mzx}} = [(\Delta x E_{12}^x + Z_{mzy}\Delta z H_{12}^z) - (\Delta x E_1^x - Z_{mzy}\Delta z H_1^z)]^{(n-1/2)}$	$2Z_0\frac{\Delta z H_{zx}^{(n)}}{\bar{D}_{zx}A_{mzx}} = 2Z_0\frac{\Delta z H_{zx}^{(n-1)}}{\bar{D}_{zx}A'_{mzx}}$
Implicit part (from $n\Delta t$ to $(n+1/2)\Delta t$)	Coefficients
$\frac{2\Delta x E_{xz}^{(n)}}{A'_{exz}} + \frac{2\Delta x E_{xy}^{(n)}}{A'_{exy}} = [(\Delta x E_2^x - Z_{exz}\Delta y H_2^y) + (\Delta x E_9^x + Z_{exz}\Delta y H_9^y)]^{(n+1/2)}$	$\bar{C}_{ij} = \frac{s\Delta i}{\varepsilon_i\alpha_j\Delta j\Delta k}$
$\frac{2\Delta y E_{yx}^{(n)}}{A'_{eyx}} + \frac{2\Delta y E_{yz}^{(n)}}{A'_{eyz}} = [(\Delta y E_3^y - Z_{eyx}\Delta z H_3^z) + (\Delta y E_{11}^y + Z_{eyx}\Delta z H_{11}^z)]^{(n+1/2)}$	$Z_{eij} = Z_0\bar{C}_{ij}$
$\frac{2\Delta z E_{zy}^{(n)}}{A'_{ezy}} + \frac{2\Delta z E_{zx}^{(n)}}{A'_{ezx}} = [(\Delta z E_5^z - Z_{ezy}\Delta x H_5^x) + (\Delta z E_7^z + Z_{ezy}\Delta x H_7^x)]^{(n+1/2)}$	$A_{eij} = \frac{4}{4+R_{eij}}$
$2Z_0\frac{\Delta x H_{xy}^{(n)}}{A'_{mxy}\bar{D}_{xy}} + 2Z_0\frac{Z_{mxy}}{Z_{mxz}}\frac{\Delta x H_{xz}^{(n)}}{A'_{mxz}\bar{D}_{xz}} = [-(\Delta z E_5^z - Z_{mxy}\Delta x H_5^x) + (\Delta z E_7^z + Z_{mxy}\Delta x H_7^x)]^{(n+1/2)}$	$A'_{eij} = \frac{4}{4-R_{eij}}$
$2Z_0\frac{\Delta y H_{yz}^{(n)}}{A'_{myz}\bar{D}_{yz}} + 2Z_0\frac{Z_{myz}}{Z_{myx}}\frac{\Delta y H_{yx}^{(n)}}{A'_{myx}\bar{D}_{yx}} = [-(\Delta x E_2^x - Z_{myz}\Delta y H_2^y) + (\Delta x E_9^x + Z_{myz}\Delta y H_9^y)]^{(n+1/2)}$	$R_{eij} = Z_0 s\frac{\sigma_{ej}}{\varepsilon_i}$
$2Z_0\frac{\Delta z H_{zx}^{(n)}}{A'_{mzx}\bar{D}_{zx}} + 2Z_0\frac{Z_{mzx}}{Z_{mzy}}\frac{\Delta z H_{zy}^{(n)}}{A'_{mzy}\bar{D}_{zy}} = [-(\Delta y E_3^y - Z_{mzx}\Delta z H_3^{zx}) + (\Delta y E_{11}^y + Z_{mzx}\Delta z H_{11}^{zx})]^{(n+1/2)}$	$s = 2c_0\Delta t$

components per cell need to be stored which represents a memory economy of a factor 2 compared to the standard PML-TLM scheme (24 voltages per cell).

4. RESULTS

PML are tested as wideband matched load of the rectangular waveguide depicted in Figure 2. The waveguide is excited by the TE_{10} mode over a wide frequency band: from 0 to 30 GHz. This corresponds to the upper dispersion limit of the TLM method generally used ($\Delta l/\lambda \sim 0.1$). This canonical case is very relevant in testing absorbing conditions. Indeed, the TE_{10} mode can be

Table II. Summary of PML SS-TLM updating equations for step 2.

Explicit part (from $(n+\frac{1}{2})\Delta t$ to $(n+1)\Delta t$)	
$\frac{2\Delta x E_{xz}^{(n+1)}}{A_{\mathrm{ex}z}} + \frac{2\Delta x E_{xy}^{(n+1)}}{A_{\mathrm{ex}y}} = [(\Delta x E_2^x + Z_{\mathrm{ex}z}\Delta y H_2^y) + (\Delta x E_9^x - Z_{\mathrm{ex}z}\Delta y H_9^y)]^{(n+1/2)}$	$\frac{2\Delta x E_{xy}^{(n+1)}}{A_{\mathrm{ex}y}} = \frac{2\Delta x E_{xy}^{(n)}}{A'_{\mathrm{ex}y}}$
$\frac{2\Delta y E_{yx}^{(n+1)}}{A_{\mathrm{ey}x}} + \frac{2\Delta y E_{yz}^{(n+1)}}{A_{\mathrm{ey}z}} = [(\Delta y E_3^y + Z_{\mathrm{ey}x}\Delta z H_3^z) + (\Delta y E_{11}^y - Z_{\mathrm{ey}x}\Delta z H_{11}^z)]^{(n+1/2)}$	$\frac{2\Delta y E_{yz}^{(n+1)}}{A_{\mathrm{ey}z}} = \frac{2\Delta y E_{yz}^{(n)}}{A'_{\mathrm{ey}z}}$
$\frac{2\Delta z E_{zy}^{(n+1)}}{A_{\mathrm{ez}y}} + \frac{2\Delta z E_{zx}^{(n+1)}}{A_{\mathrm{ez}x}} = [(\Delta z E_5^z + Z_{\mathrm{ez}y}\Delta x H_5^x) + (\Delta z E_7^z - Z_{\mathrm{ez}y}\Delta x H_7^x)]^{(n+1/2)}$	$\frac{2\Delta z E_{zx}^{(n+1)}}{A_{\mathrm{ez}x}} = \frac{2\Delta z E_{zx}^{(n)}}{A'_{\mathrm{ez}x}}$
$2Z_0\frac{\Delta x H_{xy}^{(n+1)}}{\bar{D}_{xy}A_{mxy}} + \frac{Z_{mxy}}{Z_{mxz}}2Z_0\frac{\Delta x H_{xz}^{(n+1)}}{\bar{D}_{xz}A_{mxz}} = [(\Delta z E_5^z + Z_{mxy}\Delta x H_5^x) - (\Delta z E_7^z - Z_{mxy}\Delta x H_7^x)]^{(n+1/2)}$	$2Z_0\frac{\Delta x H_{xz}^{(n+1)}}{\bar{D}_{xz}A_{mxz}} = 2Z_0\frac{\Delta x H_{xz}^{(n)}}{\bar{D}_{xz}A'_{mxz}}$
$2Z_0\frac{\Delta y H_{yz}^{(n+1)}}{\bar{D}_{yz}A_{myz}} + \frac{Z_{myz}}{Z_{myx}}2Z_0\frac{\Delta y H_{yx}^{(n+1)}}{\bar{D}_{yx}A_{myx}} = [(\Delta x E_2^x + Z_{myz}\Delta y H_2^y) - (\Delta x E_9^x - Z_{myz}\Delta y H_9^y)]^{(n+1/2)}$	$2Z_0\frac{\Delta y H_{yx}^{(n+1)}}{\bar{D}_{yx}A_{myx}} = 2Z_0\frac{\Delta y H_{yx}^{(n)}}{\bar{D}_{yx}A'_{myx}}$
$2Z_0\frac{\Delta z H_{zx}^{(n+1)}}{A_{mzx}\bar{D}_{zx}} + \frac{Z_{mzx}}{Z_{mzy}}2Z_0\frac{\Delta z H_{zy}^{(n+1)}}{A_{mzy}\bar{D}_{zy}} = [(\Delta y E_3^y + Z_{mzx}\Delta z H_3^z) - (\Delta y E_{11}^y - Z_{mzx}\Delta z H_{11}^z)]^{(n+1/2)}$	$2Z_0\frac{\Delta z H_{zy}^{(n+1)}}{\bar{D}_{zy}A_{mzy}} = 2Z_0\frac{\Delta z H_{zy}^{(n)}}{\bar{D}_{zy}A'_{mzy}}$
Implicit part (from $(n+1)\Delta t$ to $(n+\frac{3}{2})\Delta t$)	**Coefficients**
$\frac{2\Delta x E_{xy}^{(n+1)}}{A'_{\mathrm{ex}y}} + \frac{2\Delta x E_{xz}^{(n+1)}}{A'_{\mathrm{ex}z}} = [(\Delta x E_1^x + Z_{\mathrm{ex}y}\Delta z H_1^z) + (\Delta x E_{12}^x - Z_{\mathrm{ex}y}\Delta z H_{12}^z)]^{(n+3/2)}$	$\bar{D}_{ij} = \frac{s\Delta i}{\mu_i\alpha_j\Delta j\Delta k}$
$\frac{2\Delta y E_{yz}^{(n+1)}}{A'_{\mathrm{ey}z}} + \frac{2\Delta y E_{yx}^{(n+1)}}{A'_{\mathrm{ey}x}} = [(\Delta y E_4^y + Z_{\mathrm{ey}z}\Delta x H_4^x) + (\Delta y E_8^y - Z_{\mathrm{ey}z}\Delta x H_8^x)]^{(n+3/2)}$	$Z_{mij} = \frac{Z_0}{\bar{D}_{ij}}$
$\frac{2\Delta z E_{zx}^{(n+1)}}{A'_{\mathrm{ez}x}} + \frac{2\Delta z E_{zy}^{(n+1)}}{A'_{\mathrm{ez}y}} = [(\Delta z E_6^z + Z_{\mathrm{ez}x}\Delta y H_6^y) + (\Delta z E_{10}^z - Z_{\mathrm{ez}x}\Delta y H_{10}^y)]^{(n+3/2)}$	$A_{mij} = \frac{4}{4+R_{mij}}$
$2Z_0\frac{\Delta x H_{xz}^{(n+1)}}{A'_{mxz}\bar{D}_{xz}} + 2Z_0\frac{Z_{mxz}}{Z_{mxy}}\frac{\Delta x H_{xy}^{(n+1)}}{A'_{mxy}\bar{D}_{xy}} = [-(\Delta y E_8^y - Z_{mxz}\Delta x H_8^x) + (\Delta y E_4^y + Z_{mxz}\Delta x H_4^x)]^{(n+3/2)}$	$A'_{mij} = \frac{4}{4-R_{mij}}$
$2Z_0\frac{\Delta y H_{yx}^{(n+1)}}{A'_{myx}\bar{D}_{yx}} + 2Z_0\frac{Z_{myx}}{Z_{myz}}\frac{\Delta y H_{yz}^{(n+1)}}{A'_{myz}\bar{D}_{yz}} = [-(\Delta z E_{10}^z - Z_{myx}\Delta y H_{10}^y) + (\Delta z E_6^z + Z_{myx}\Delta y H_6^y)]^{(n+3/2)}$	$R_{mij} = s\frac{\sigma_{mj}}{Z_0\mu_i}$
$2Z_0\frac{\Delta z H_{zy}^{(n+1)}}{A'_{mzy}\bar{D}_{zy}} + 2Z_0\frac{Z_{mzy}}{Z_{mzx}}\frac{\Delta z H_{zx}^{(n+1)}}{A'_{mzx}\bar{D}_{zx}} = [-(\Delta x E_{12}^x - Z_{mzy}\Delta z H_{12}^z) + (\Delta x E_1^x + Z_{mzy}\Delta z H_1^z)]^{(n+3/2)}$	$s = 2c_0\Delta t$

seen as superposition of plane waves at all cases of incidence. In addition, since evanescent waves are generated below cutoff ABC are also tested in the presence of such waves. The wide-band reflection coefficient on PML layers is calculated in a single run using the technique described in Reference [12].

4.1. Profile optimization

The SS-TLM PML scheme is first tested at maximum time-step of TLM ($\Delta t_{\max}$) to obtain an optimized layer. Thus, optimal conductivities (i.e. σ_{ez} and σ_{mz}) and α_z profile have to be

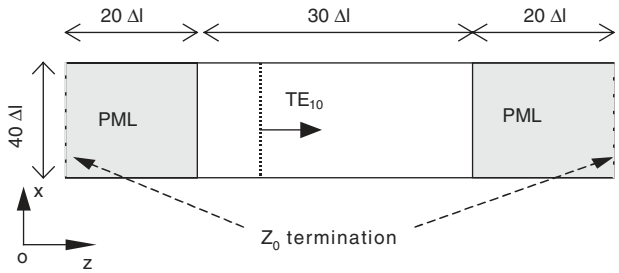

Figure 2. Geometry of the numerical test: a rectangular waveguide (cross-section $40 \times 20\Delta l$, $\Delta l = 1$ mm) truncated with a 20 cells PML and wideband excited with the TE_{10} mode (cutoff frequency: 3.75 GHz). PML are terminated with Z_0 impedance.

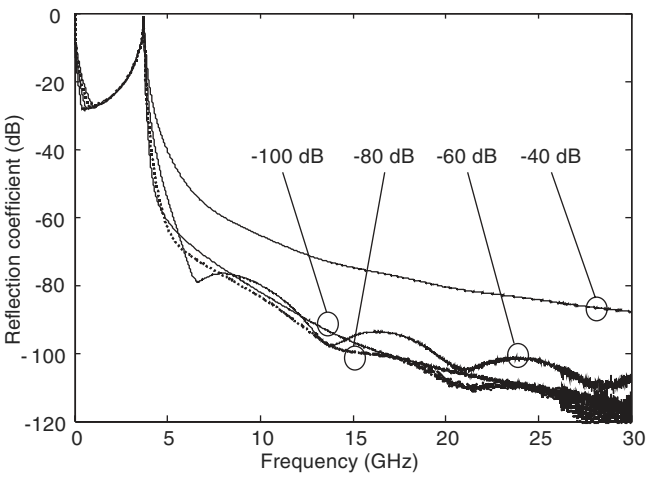

Figure 3. Reflection coefficient in a rectangular waveguide (Figure 2). $F_z = 1$ and several R_{prop} values (parabolic profile).

determined to obtain the best absorption. Note that, in the following, the PML layer is characterized by its theoretical reflection coefficient at normal incidence (R_{prop}) and F_z a coefficient that represents damping added to evanescent waves (for further details see Reference [8]).

The first test is performed without additional evanescent wave damping ($F_z = 1$) for several values of R_{prop}. The conductivity profile used is parabolic since it is known as providing the best absorption (see for instance Reference [8]). Results depicted in Figure 3 are decomposed into two parts: propagating and evanescent waves. The limit between both parts corresponds to the cutoff frequency (3.75 GHz) where the reflection coefficient computed is 0 dB because waves impinge on the layer with an angle of 90°. One can observe that with $R_{\text{prop}} = -40$ dB, a reflection coefficient better than -60 dB is achieved for propagating waves. This is due to the attenuation added by the Z_0 impedance that terminates the PML layer mesh. Furthermore, the reflection level decreases with R_{prop} value down to -80 dB. For lower values, reflection starts to increase because of the numerical reflection due to high values of conductivity at the interface

between the classical and the PML medium. Thus, the optimal profile is achieved with $R_{\text{prop}} = -80$ dB and the corresponding reflection is around -100 dB.

From a physical point of view, the computed reflection coefficient for evanescent waves rather corresponds to a perturbation of the spatial repartition of stored energy. The optimal PML layer should then provide a value of this perturbation as low as possible. Since the layer tested in Figure 3 does not add any attenuation to evanescent energy the perturbation observed is mainly produced by the layer truncation. Note that the perturbation can be reduced by using thicker layers as evanescent waves are naturally damped. However, more computational effort is required in this case.

Optimal layer performance is obtained by adding evanescent wave damping (i.e. values of F_z larger than unity). The corresponding α_z profile used is defined in Reference [8]. As shown by Figure 4, evanescent waves perturbation decreases down to -80 dB with F_z equal to 4. On the other hand, since α_z acts as a sub-permittivity term, the dispersion of the technique increases and the reflection of propagating waves follows the same trend. Thus, the optimal profile is obtained with R_{prop} and F_z equal to -80 dB and 4, respectively. This achieves a reflection coefficient of -80 dB with both propagating and evanescent waves.

4.2. Comparison with TLM

TLM PML and SS-TLM PML are compared at TLM maximum time-step. The profile used is the optimum one obtained with SS-TLM. Results are depicted in Figure 5. It should be noted that SS-TLM provides less reflection than TLM: a 20-dB improvement is achieved for evanescent waves, and the same reduction is observed for propagating waves at the centre of the band. However, both techniques provide the same level of reflection in the upper part of the spectrum.

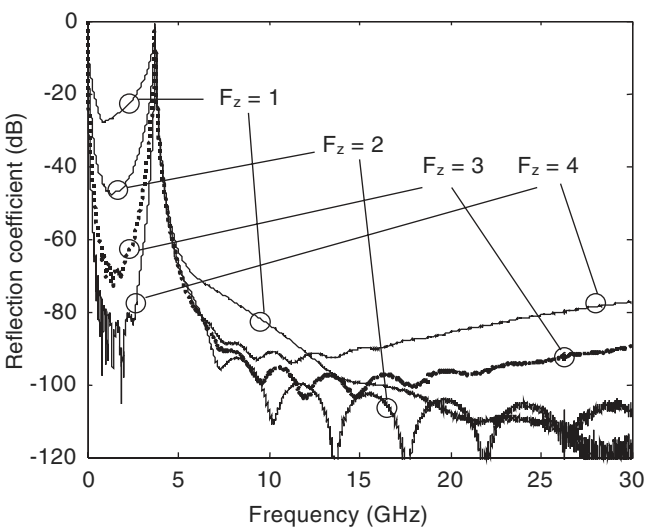

Figure 4. Reflection coefficient in a rectangular waveguide (Figure 2). Several F_z values and $R_{\text{prop}} = -80$ dB (parabolic profile).

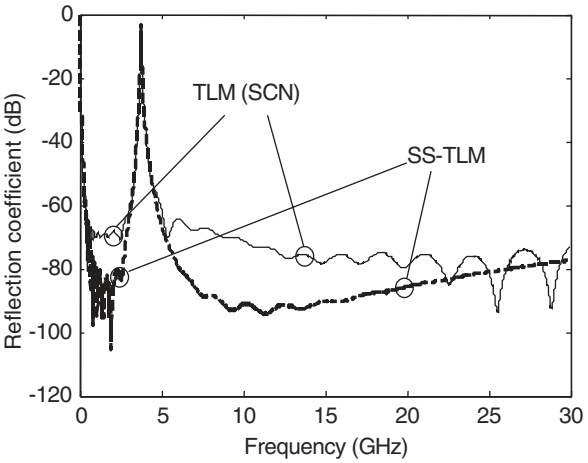

Figure 5. Reflection coefficient in a rectangular waveguide (Figure 2). $F_z = 4$ and $R_{\text{prop}} = -80$ dB (parabolic profile) with TLM and SS-TLM schemes.

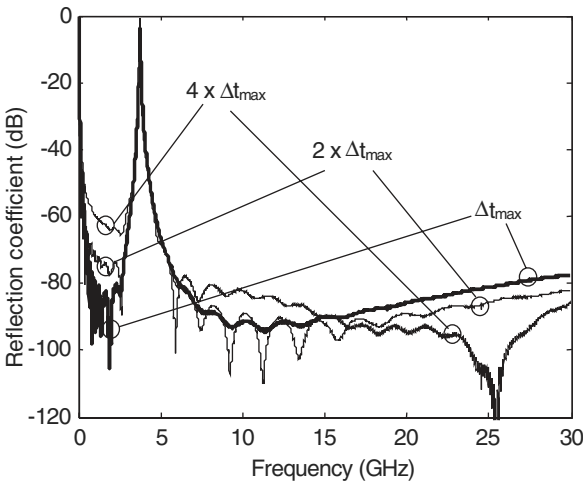

Figure 6. Reflection coefficient in a rectangular waveguide (Figure 2). $F_z = 4$ and $R_{\text{prop}} = -80$ dB (parabolic profile) with several values of time-step ($\Delta t_{\max}$ is the maximum time-step of TLM classical scheme).

4.3. Time-step effect

Finally, since SS-TLM is to be used at a time-step larger than that of TLM ($\Delta t_{\max}$), the optimal layer is tested in these conditions. One can note from results shown in Figure 6 that the layer performances decrease slowly with time-step. Even with a time-step four times larger than $\Delta t_{\max}$, the performance are still excellent (-65 dB for evanescent waves and -80 dB for propagating

waves). This result is very surprising because SS-TLM dispersion has been shown to rapidly increases with the time-step [4]. It can be concluded that this dispersion slightly affects the efficiency of PML layers. As a consequence, PML layer is very well-adapted to SS-TLM.

4.4. Stability

A key issue of the PML technique in TLM is the stability of the layers. A lot of work has already been driven to achieve long-term stability of the layers [8, 13, 14]. Many authors have suspected the presence of TLM spurious modes to be at the origin of the problem. Since it can be shown that spurious modes do not exist with SS-TLM [9], one may conclude that the associated PML technique will be stable. A theoretical proof of the stability is rather involved and can be done only numerically. Thus, a numerical experiment is preferred as it can be chosen for relevant cases where numerical instabilities occurred with standard TLM algorithm (see, for instance References [8] and [13]). For instance, consider the benchmark geometry depicted in Figure 7. It is composed of a rectangular waveguide terminated in one end by a perfect electric wall and in the other end by a PML layer without additional evanescent waves damping ($F_z = 1$). The layer is backed with a perfect electric conductor. The waveguide is excited by the TE_{10} mode. Between the excitation plane and the PML layer, a capacitive iris is inserted. Thus, the problem is a full 3D simulation. This configuration is highly unstable with TLM (see Reference [8]) since the instability appears after 600 iterations.

The same simulation performed with SS-TLM using up to 10^5 iterations shows no instability. Numerous simulations involving complex structures have further confirmed this observation. This corroborates the assertion that spurious modes have a predominant role in the instabilities observed with standard TLM-PML schemes.

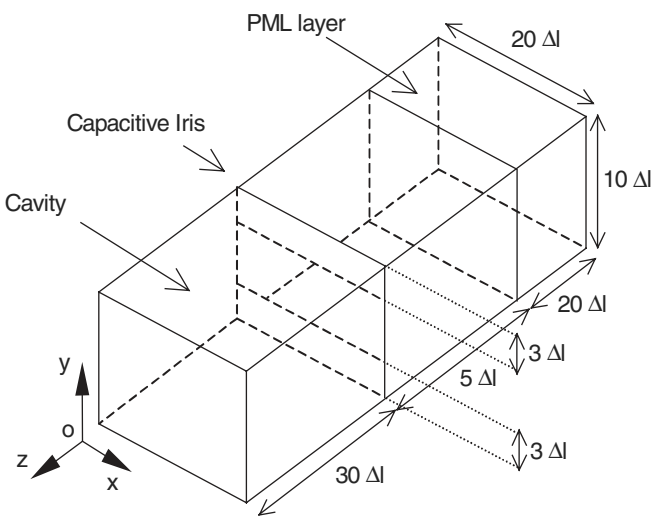

Figure 7. Test configuration for PML scheme stability ($\Delta l = 1$ mm). PML parameters: $R_{\text{prop}} = -80$ dB, parabolic profile, $F_z = 1$, backed with a perfect electric wall.

4.5. *Antenna simulation*

The last validation example was performed by simulating a class of miniaturized microstrip antennas [15] with inhomogeneous substrate (Figure 8).

It is composed of an air-like dielectric substrate that guaranties optimum radiation efficiency. By inserting a piece of higher permittivity substrate underneath the patch, the size of the antenna can be reduced. It should be noted that this kind of geometry requires a full 3D technique which can be easily provided by volumic techniques such as TLM.

This antenna was already simulated using TLM (see Reference [8]). However, to obtain the result in a reasonable time, the 50-μm polypropylene film that is needed to stick the conductor on the substrate was ignored. If one wants to take into account this film, a high-density variable-mesh has to be used. The basic cell-size chosen is $\Delta l = 0.8$ mm. Hence, the density of the mesh has to be 16 times larger to correctly approximate the polypropylene film.

The simulation was performed both with SS-TLM and SCN-TLM. The volume was discretized by $25 \times 47 \times 91$ cells using irregular mesh. The PML layers were 15 cells thick (parabolic profile, $R_{\text{prop}} = -80$ dB, $F_z = 3$). Using the meshing strategy described in Reference [4], the SS-TLM time-step was based on the largest cell size. Note that a time-step 32 times smaller was required for SCN-TLM computations as the smallest cell imposes the maximum time-step. The reflection coefficients obtained are depicted in Figure 9 where they are compared to measurement.

Results show that SS-TLM is in excellent agreement with measurements (for bandwidth, resonance frequency and matching). Also, TLM provides a rather large error (more than 4% for resonance frequency). This is due to the fact that a large part of the mesh is computed at a time-step much smaller than the maximum time-step that normally prevails. Thus, dispersion is increased (see Reference [4]) and significantly affects the accuracy of the results. It is noteworthy to mention that the above results were made using the shortest excitation possible to reduce TLM computation time. Still, it requires a simulation 17 times longer than SS-TLM.

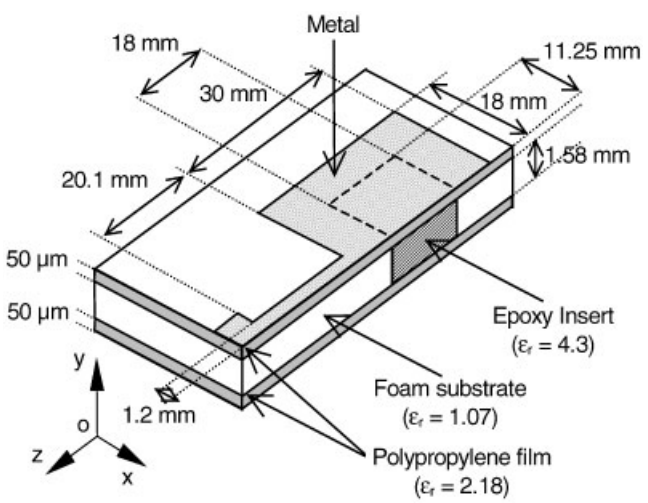

Figure 8. One half of the microstrip antenna on a locally non-homogeneous substrate.

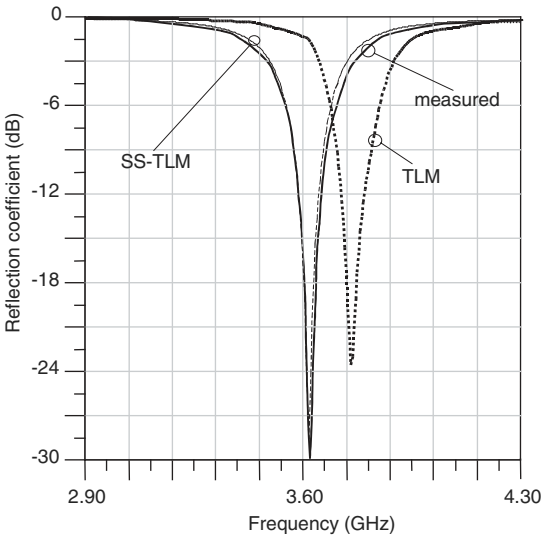

Figure 9. Reflection coefficient obtained with the antenna depicted in Figure 8. Comparison between SS-TLM, TLM and measurements.

In addition, if the thin propylene film is ignored, TLM results are far more accurate (see Reference [8]) but not as accurate as SS-TLM results provided here. Hence, to get an accurate result by taking into account the film with classical TLM, one has to use a much smaller basic cell consequently increasing both the memory and the CPU time required.

5. CONCLUSION

An extended PML formulation based on Berenger's work has been implemented for the SS-TLM scheme. Results show that the new PML technique provides low reflection level for both propagating and evanescent waves. A comparison with classical PML-TLM was carried out showing SS-TLM advantages. Furthermore, the accuracy of the new scheme does not seem to degrade significantly when the time-step increases. This provides a great advantage over standard TLM when irregular meshing is used. In addition, long-term stability seems to be achieved which is a key feature in TLM simulation with PML. Finally, the SS-TLM method is applied to the analysis of a complex antenna showing a gain in CPU time larger than one order of magnitude compared to SCN-TLM.

REFERENCES

1. Namiki T. A new FDTD algorithm based on Alternating-Direction implicit method. *IEEE Transactions on Microwave Theory and Techniques* 1999; **47**(10):2003–2007.
2. Zheng F, Chen Z, Zhang J. Toward the development of a three-dimensional unconditionally stable finite-difference time-domain method. *IEEE Transactions on Microwave Theory and Techniques* 2000; **48**(9):1550–1558.
3. Le Maguer S, Ney MM. Towards a new low-computer-cost 3D-TLM scheme (ADI-TLM). *4th International Workshop on Computational Electromagnetics in the Time-Domain and Related Techniques* (*TLM-FDTD*), Nottingham, UK, September 2001; 120–125.

4. Le Maguer S, Ney MM. Split Step TLM (SS-TLM) for efficient electromagnetic simulation of small heterogenous apertures. *Proceedings of EMC Symposium*, Zürich 52I6, February 2003; 275–278.
5. Marchuk GI. Splitting and Alternating Direction Methods. *Handbook of Numerical Analysis*, Ciarlet PG, Lions JL (eds), vol. 1. North Holland: Amsterdam, 1990.
6. Peña N, Ney MM. A general formulation of a three-dimensional TLM condensed node with the modelling of electric and magnetic losses and current sources. *ACES'96 Conference Proceedings*, 1996; 262–269.
7. Bérenger JP. A perfectly matched Layer for the absorption of electromagnetic waves. *Journal of Computational Physics* 1994; **144**(2):110–117.
8. Le Maguer S, Ney MM. Extended PML-TLM: An efficient approach for full-wave analysis of open structures. *International Journal of Numerical Modelling* 2001; **14**:129–144.
9. Le Maguer S, Peden A, Bourreau D, Ney MM. Split-step TLM (SS-TLM): a new scheme for accelerating electromagnetic field simulation. *IEEE Transactions on Microwave Theory and Techniques*, to be published.
10. Gedney SD. An anisotropic perfectly matched layer absorbing medium for the truncation of FDTD lattices. *IEEE Transactions on AP* 1996; **44**(12):1630–1639.
11. Johns PB. A symmetrical condensed node for the TLM method. *IEEE Transactions on Microwave Theory and Techniques* 1987; **35**(4):370–377.
12. Christopoulos C, Smart CJ. Microwave application of TLM modelling techniques. *International Journal of Microwave and Millimeter-Wave Computer-Aided Engineering* 1996; **6**(1):26–35.
13. Le Maguer S, Peña N, Ney MM. Matched absorbing medium techniques for full-wave TLM simulation of microwave and millimeter wave components. *Annales des télécommunications* 1998; **53**(3–4):115–129.
14. Kang TW, Christopoulos C, Paul J. Implementation of the stretched coordinate-based PML waveguide structures in TLM. *5th CEM-TD Workshop*, Halifax, Nova Scotia, 2003; 7–9.
15. Lattard H, Le Maguer S, ToutainY, Coupez JP, Person C. High performance miniaturized microstrip antennas on locally non-homogeneous substrate. *29th European Microwave Conference*, Munich, vol. **3**. 1999; 67–70.